Synthesis of a mixed-metal spinel, $NiMn_2O_4$, through site-selective substitution in MOF, $[(NiMn_2)\{C_6H_3(COO)_3\}_2]$: synthesis, structure and magnetic studies

Debajit Sarma, Partha Mahata and Srinivasan Natarajan*

Framework Solids Laboratory, Solid State and Structural Chemistry Unit, Indian Institute of Science, Bangalore 560 012, India

A mixed-metal metal–organic framework (MOF) compound $[NiMn_2\{C_6H_3(COO)_3\}_2]$, I, is prepared hydrothermally by replacing one of the octahedral Mn^{2+} ions in $[Mn_3\{C_6H_3(COO)_3\}_2]$ by Ni^{2+} ions. Magnetic studies on I suggest antiferromagnetic interactions with weak canted antiferromagnetism below 8 K. On heating in flowing air I transforms to $NiMn_2O_4$ spinel at low temperature (T < 400°C). The thermal decomposition of I at different temperatures results in $NiMn_2O_4$ with particle sizes in the nano regime. The nanoparticle nature of $NiMn_2O_4$ was confirmed using PXRD and TEM studies. Magnetic studies on the nanoparticles of $NiMn_2O_4$ indicate ferrimagnetism. The transition temperature of $NiMn_2O_4$ nanoparticles exhibits a direct correlation with the particle size. This study highlights the usefulness of MOF compound as a single-source precursor for the preparation of important ceramic oxides with better control on the stoichiometry and particle size.

Keywords: Magnetic studies, metal–organic framework, mixed-metal spinel, nanoparticles.

SPINEL oxides with the general formula AB_2O_4 are an important family of compounds exhibiting interesting physical and chemical properties[1,2]. The cations in a spinel structure generally occupy tetrahedral (A cations) or the octahedral (B cations) voids created by the cubic close packed arrangement of the oxide ions[1–3]. The continued interest in spinel-based compounds stems from their electronic structure, which gives rise to interesting electrical[4], optical[5] and magnetic[6] properties. Manipulation of the cations and their occupancy at the respective crystallographic positions in the spinel structure lead to the discovery of many technologically important compounds, which find use in multiferroics[7], thermoelectrics[8], superconductivity[9], colossal magnetoresistivity (CMR)[10] and spin-based electronics[11]. Of the many spinel phases known, nickel manganate ($NiMn_2O_4$) is important. It has an inverse spinel structure, where the A cation (Ni) occupies the octahedral voids. $NiMn_2O_4$ exhibits negative thermal coefficient and finds use in thermistors[12].

The synthesis of mixed-metal oxides has been explored extensively in the literature[1,2]. The spinel phases have been prepared using a wide variety of techniques such as coprecipitation[13], sol–gel[14], combustion synthesis[15], hydrothermal method[16], high-energy ball-milling[17], thermal plasma synthesis[18] and spray pyrolysis on a hot surface of metal nitrate solutions[19]. Single-source precursors have also attracted considerable interest for the preparation of mixed-metal oxides for their precise control over the stoichiometry[1]. Most of the mixed oxides are synthesized by employing the ceramic route with temperatures in excess of 1000°C. Single-source precursors, on the other hand, have been shown to form ceramic oxides at a much lower temperature[1,2]. This approach provides better control over the stoichiometry of the ceramic oxides and has been successfully employed in the preparation of multi-component mixed-metal oxides[1,20,21].

The rapid advances in the area of inorganic–organic hybrids, especially metal–organic framework (MOF) compounds provide new vistas in the area of materials chemistry[22–24]. Though MOF compounds have been employed similar to the traditional porous framework compounds in the areas of catalysis, sorption and separation processes[25], recent research indicates that they are amenable for chemical manipulations, leading to interesting properties[26,27]. The MOF compounds have metal cations connected by the carboxylate anions. Decomposition of the MOF compounds generally results in simple metal-oxide powders, as the organics leave the system as CO and CO_2 under atmospheric conditions. This provides the basis to use MOF compounds as a useful single-source precursor for the synthesis of ceramic oxides. This approach also provides an added impetus to study the MOF compounds. In addition to preparing the new MOF compounds exhibiting novel structures, one can now structurally manipulate them to form interesting oxide materials. We have employed this strategy successfully in the preparation of perovskite and spinel oxides[20,28]. It may be noted that the use of single-source precursors generally reduces the synthesis temperature of the ceramic oxides.

*For correspondence. (e-mail: snatarajan@sscu.iisc.ernet.in)

Incorporation of more than one transition element in a homometallic MOF poses a challenge for the synthetic chemists. Mixed-metal MOF compounds with more than one transition element in the same structure are rare[29]. The general approach towards this goal involves the use of a coordinatively saturated metal as part of the ligand (metal porphyrin-based ligands), post-synthetic modification[30] and direct and partial replacement of the transition metal in a homometallic MOF by controlling the stoichiometry of the reaction mixture. Matzger and coworkers[31] exploited the geometrical preference of the metal ions in a MOF for selective incorporation of a transition metal within a homometallic MOF. We have also employed this strategy recently[28], by selectively incorporating Co^{2+} ions at the octahedral sites in $[Mn_3\{C_6H_3(COO)_3\}_2]$. The MOF, $[Mn_3\{C_6H_3(COO)_3\}_2]$, has both trigonal prismatic coordination as well as octahedral coordination for the Mn^{2+} ions[32]. The Co^{2+} ions generally prefer octahedral coordination, which was employed for the partial substitution in our earlier study[28]. In continuation of this work[28], we have now selectively replaced the octahedral Mn^{2+} by Ni^{2+} ions forming $[NiMn_2\{C_6H_3(COO)_3\}_2]$, **I**. On heating **I**, transforms to a nickel manganate spinel, $NiMn_2O_4$ at around 400°C. In this article, we present the synthesis, structure and magnetic properties of the Ni^{2+}-substituted MOF, **I**, along with the formation of the $NiMn_2O_4$ spinel phase with particle sizes in the nano-regime range. As part of the investigations, the microscopic as well as magnetic properties of the $NiMn_2O_4$ parent heterometallic MOF (**I**) and the spinel $NiMn_2O_4$ nanoparticles have also been studied.

Experimental section

Synthesis

In 8 ml of water, $Mn(OAc)_2{\cdot}4H_2O$ (0.1618 g, 0.66 mM), $Ni(OAc)_2.4H_2O$ (0.0822 g, 0.33 mM), 1,2,4-benzenetricarboxylic acid (0.2101 g, 1 mM), imidazole (0.0681 g, 1 mM) and KOH (0.1122 g, 2 mM) were mixed thoroughly and heated in a PTFE-lined stainless steel autoclave at 220°C for 24 h. The resulting product contains light green-coloured powders of **I** (yield 68%, based on the metal). The products were filtered, washed with deionized water and dried at ambient conditions. Elemental analysis Calcd (%) for **I**: Anal. Calcd: C, 37.10; H, 1.04. Found: C, 37.43; H, 1.21.

*Initial characterizations of **I***

Powder X-ray diffraction (PXRD) patterns of **I** were recorded on well-ground samples (2θ range 5–50°) employing CuKα radiation (Philips X'pert) (Electronic Supplementary Information (ESI), Figure S1; available online). The XRD patterns suggested that the product phase was consistent with the simulated XRD pattern generated using the single-crystal structure of the parent homometallic MOF, $[Mn_3\{C_6H_3(COO)_3\}_2]$. The IR spectrum was recorded at ambient temperature (25°C) on a KBr pellet (Perkin Elmer, SPECTRUM 1000) (ESI, Figure S2; available online). IR (KBr): $\gamma_s(C–H)_{aromatic}$ = 2983 cm^{-1}, $\gamma_s(C{=}O)$ = 1593 cm^{-1}, $\delta(COO)$ = 1405 cm^{-1}, $\gamma_s(C–C)_{skeletal}$ = 937 cm^{-1} and $\delta(CH_{aromatic})_{out\ of\ plane}$ = 763 cm^{-1}. The thermogravimetric analysis (TGA) (Metler-Toledo) in oxygen atmosphere (flow rate = 20 ml/min) was carried out in the temperature range 30–850°C (heating rate = 5°C/min) (ESI, Figure S3; available online). The TGA studies exhibited weight losses in the temperature range 380–690°C. The total observed weight loss of 61.9% corresponds well with the loss of the carboxylate molecules (calc. 60.1%). The final calcined product was found to be crystalline by PXRD and corresponds to the spinel phase, $NiMn_2O_4$ (JCPDS: 84-0542).

The unit cell parameters for **I** were obtained from the PXRD pattern by the Le Bail method (ESI, Table S1; available online)[33].

Spinel oxide preparation and characterization

From the TGA studies, it is clear that the compound exhibits significant weight loss in the range 380–500°C and a large tail in the range 500–690°C (ESI, Figure S3; available online). In order to establish the formation and the stability range of the nickel manganate spinel oxide, $NiMn_2O_4$, the heterometallic MOF, $[NiMn_2\{C_6H_3(COO)_3\}_2]$, was heated at different temperatures for a fixed period of time (1 h). The resulting oxide products were examined and analysed employing PXRD. The morphologies and sizes of the $NiMn_2O_4$ particles were studied using transmission electron microscopy (Hi tecnai; 300 kV) by mounting the sample on carbon-coated copper grids. Specific surface areas (Belsorp-Max) of the spinel oxides were determined by Brunauer, Emmett and Teller (BET) method, after pretreating the sample at 200°C for 4 h in dry N_2 atmosphere.

Results and discussion

*Structure of **I***

The homometallic MOF, $[Mn_3\{C_6H_3(COO)_3\}_2]$ and the Co^{2+}-substituted MOF, $[CoMn_2\{C_6H_3(COO)_3\}_2]$ were studied by us[28,32]. The pure Mn and the Co-substituted compounds form as single phasic and single crystalline products. The Ni-substituted compound on the other hand, forms only as a microcrystalline powder. We could not obtain good-quality single crystals, suitable for single-crystal XRD studies, in spite of our repeated attempts. The PXRD pattern indicated close similarity with the $[Mn_3\{C_6H_3(COO)_3\}_2]$ and the $[CoMn_2\{C_6H_3(COO)_3\}_2]$

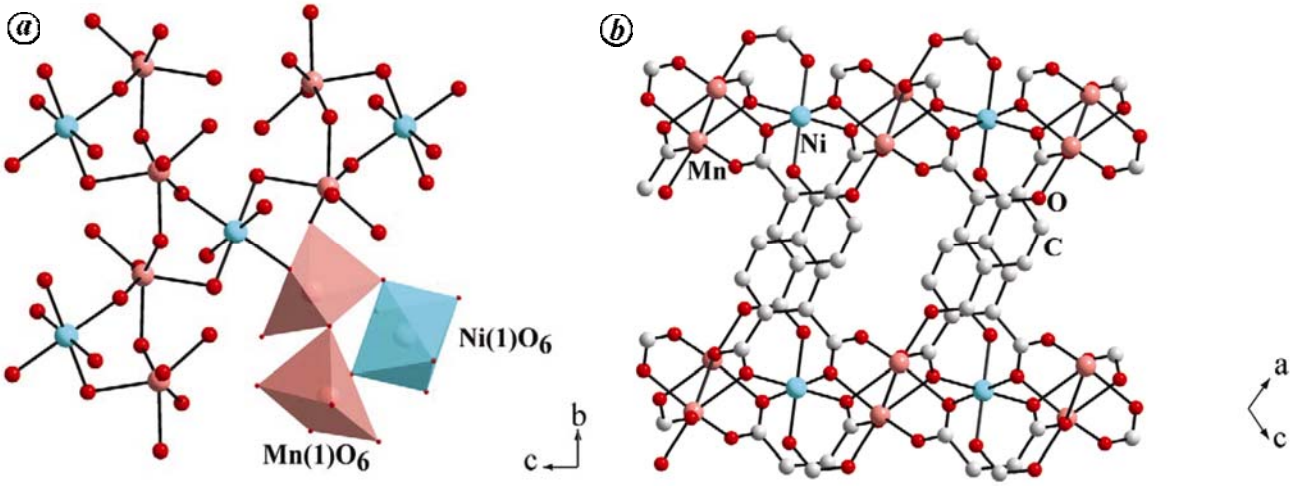

Figure 1. ***a***, A portion of the structure highlighting the connectivity between the $Ni(1)O_6$ octahedra and the $Mn(1)O_6$ trigonal prism **I**. ***b***, Connectivity between the kagome layers through the benzene carboxylate (see text).

phases (ESI, Figure S4; available online). The light green colour of the microcrystalline product is suggestive of the incorporation of Ni^{2+} ions. The ICP–OES analysis for the elements indicated a ratio of 1 : 1.94 for Ni^{2+} : Mn^{2+}. From these, one can arrive at a formula of $[NiMn_2\{C_6H_3(COO)_3\}_2]$ for compound **I**. The unit-cell parameters for **I** were obtained from the PXRD pattern employing the profile analysis fit (Le Bail method)[33]. The atomic coordinates of the parent compound, $[Mn_3\{C_6H_3(COO)_3\}_2]$[27], were employed to extract the structure factor amplitude, which was used during the structural refinement cycles. The refinement included the scale factor, the zero-point shift, the lattice parameters and the background parameters as the variables. The various parameters obtained from the refinements are listed in ESI, Table S1; for Le Bail fit see ESI, Figure S5; available online). The close similarity in the lattice parameters of **I** to the Co^{2+} substituted MOF, $[CoMn_2\{C_6H_3(COO)_3\}_2]$, suggests that the Ni^{2+} ions would be occupying the same position as the Co^{2+} ions in $[CoMn_2\{C_6H_3(COO)_3\}_2]$, which has the octahedral coordination. The structure of $[NiMn_2\{C_6H_3(COO)_3\}_2]$, **I**, is shown in Figure 1.

*Magnetic properties of **I***

Similar to the parent compound, $[Mn_3\{C_6H_3(COO)_3\}_2]$, as well as the Co^{2+}-substituted compound $[CoMn_2\{C_6H_3(COO)_3\}_2]$, the Ni^{2+}-substituted compound $[NiMn_2\{C_6H_3(COO)_3\}_2]$ also has a kagome-related structure. Kagome-related topology generates much interest due to the magnetic frustration[34,35]. Whereas the Co^{2+}-containing compound has a mixture of d^7 (Co^{2+}) and d^5 (Mn^{2+}) ions, the present Ni^{2+} compound has d^8 (Ni^{2+}) and d^5 (Mn^{2+}) ions. In addition to the differences in the crystal field splitting of the d levels (octahedral Ni^{2+} ions and trigonal prismatic Mn^{2+} ions), the differences in the total number of available electrons would also be expected to play a role in the outcome of the magnetic behaviour of $[NiMn_2\{C_6H_3(COO)_3\}_2]$. To probe the magnetic behaviour of **I**, we have carried out temperature-dependent magnetic susceptibility studies on the powdered samples of the compound using a PPMS magnetometer (Quantum Design Inc., USA).

The μ_{eff} value per $NiMn_2$ unit at room temperature was found to be 9.63 μ_B, which is considerably higher than the simple spin-only value based on noninteracting Ni^{2+} and Mn^{2+} ions (8.83 μ_B). At room temperature, the $\chi_M T$ value of **I** is 11.586 emu mol^{-1} K for two Mn^{2+} ions and one Ni^{2+} ion, which is also higher than the spin-only value ($2 \times 4.375 + 1 \times 1 = 9.75$ emu mol^{-1} K). The $\chi_M T$ value decreases as a function of temperature and reaches a minimum value of 4.33 emu mol^{-1} K at 8 K. The $\chi_M T$ value starts to increase after 8 K to reach a value of 5.59 emu mol^{-1} at 3 K (ESI, Figure S6; available online). The molar magnetic susceptibility value, χ_M of **I** increases from 0.039 emu mol^{-1} at room temperature to a maximum value of 1.87 emu mol^{-1} at 3 K (Figure 2 *a*). A plot of $1/\chi_M$ versus T in the temperature range 100–300 K, fitted to the Curie–Weiss behaviour, gave a value of 13.27 emu mol^{-1} for C, and θ_P of –44.86 K (inset, Figure 2 *a*). The negative value of θ_P indicates that the dominant exchanges between the ions could be antiferromagnetic. The field cooled (FC) and zero field cooled (ZFC) magnetic studies did not exhibit any appreciable differences in the susceptibility behaviour up to 3 K (ESI, Figure S7; available online). The magnetization (M versus H) studies also did not reveal any hysteresis-like behaviour (ESI, Figure S8; available online). In order to ascertain the possibility of spontaneous magnetization or canted antiferromagnetism in **I**, we have carried out magnetic studies at different applied DC fields. The $\chi_M T$ versus T

plots at different fields are shown in Figure 2 *b*. The studies appear to suggest that **I** exhibits a weak, spontaneous magnetization below 8 K, which shows profound field-dependency. This behaviour indicates that **I** exhibits a weak canted antiferromagnetism.

Comparison of magnetic properties of [$Mn_3\{C_6H_3(COO)_3\}_2$], [$CoMn_2\{C_6H_3(COO)_3\}_2$] and [$NiMn_2\{C_6H_3(COO)_3\}_2$]

The homometallic parent compound[32] [$Mn_3\{C_6H_3(COO)_3\}_2$], and the Co^{2+}-substituted compound [$CoMn_2\{C_6H_3(COO)_3\}_2$], exhibit canted antiferromagnetic behaviour. The present nickel-substituted compound [$NiMn_2\{C_6H_3(COO)_3\}_2$], **I**, exhibits a dominant antiferromagnetic behaviour along with the appearance of a weak canted antiferromagnetism below 8 K.

The canted antiferromagnetic behaviour of [$Mn_3\{C_6H_3(COO)_3\}_2$] and [$CoMn_2\{C_6H_3(COO)_3\}_2$] was explained invoking Dzyaloshinsky–Moriya (DM) formalism[36]. The antisymmetric DM interactions due to the presence of trigonal prismatic and octahedral coordinations for the transition metal ions, were responsible for the canted antiferromagnetism. For the Co-compound, the high single-ion anisotropy of the Co^{2+} ions also would have contributed to the canting of the spins.

The present compound, being similar to the cobalt compound, would be expected to exhibit canted antiferromagnetic behaviour. The field-dependent magnetic studies on **I** did suggest the possibility of a weak canted antiferromagnetism (< 8 K). The differences in the strength of the canted antiferromagnetic behaviour of the Co-compound and the present compound can be explained by considering the local anisotropy of the respective participating ions. The local anisotropy of Co^{2+} ion (due to first-order spin–orbit coupling) may be greater than that for the Ni^{2+} ion (due only to the second-order spin–orbit

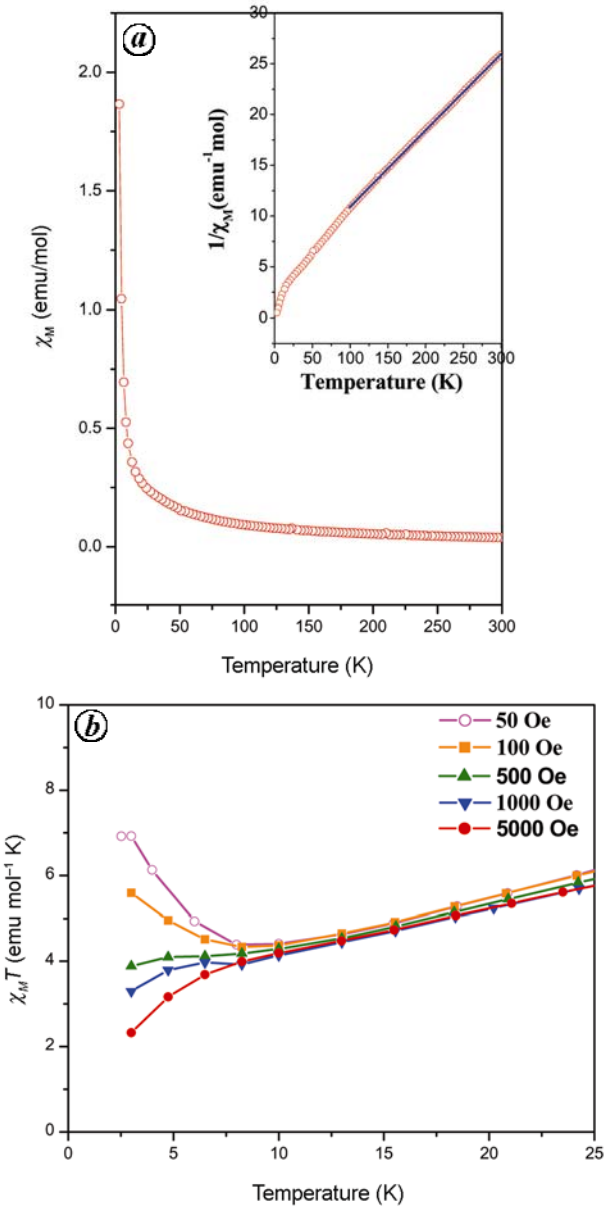

Figure 2. ***a***, Temperature variation of the molar magnetic susceptibility (χ_M) for **I**. (Inset) $1/\chi_M$ versus T behaviour. ***b***, $\chi_M T$ versus T plots for **I** at different applied DC fields.

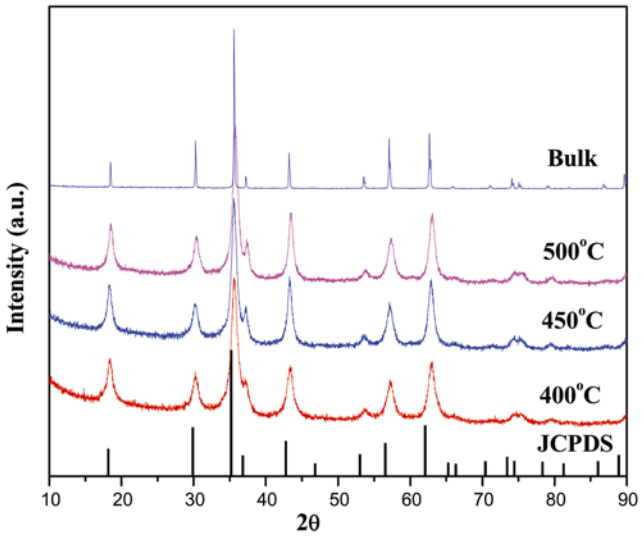

Figure 3. Powder X-ray diffraction patterns of **I** heated at different temperatures (400°C, 450°C and 500°C). The bulk $NiMn_2O_4$ along with its JCPDS patterns are also shown for comparison.

Table 1. Preparation condition and characterization of the $NiMn_2O_4$ samples

Temperature/ time	Particle size (XRD)/nm	Particle size (TEM)/nm	Surface area BET/m^2 g^{-1}
400°C/1 h	9.5	10 ± 2	81.3
450°C/1 h	11	15 ± 2	50.9
500°C/1 h	12.5	18 ± 2	39

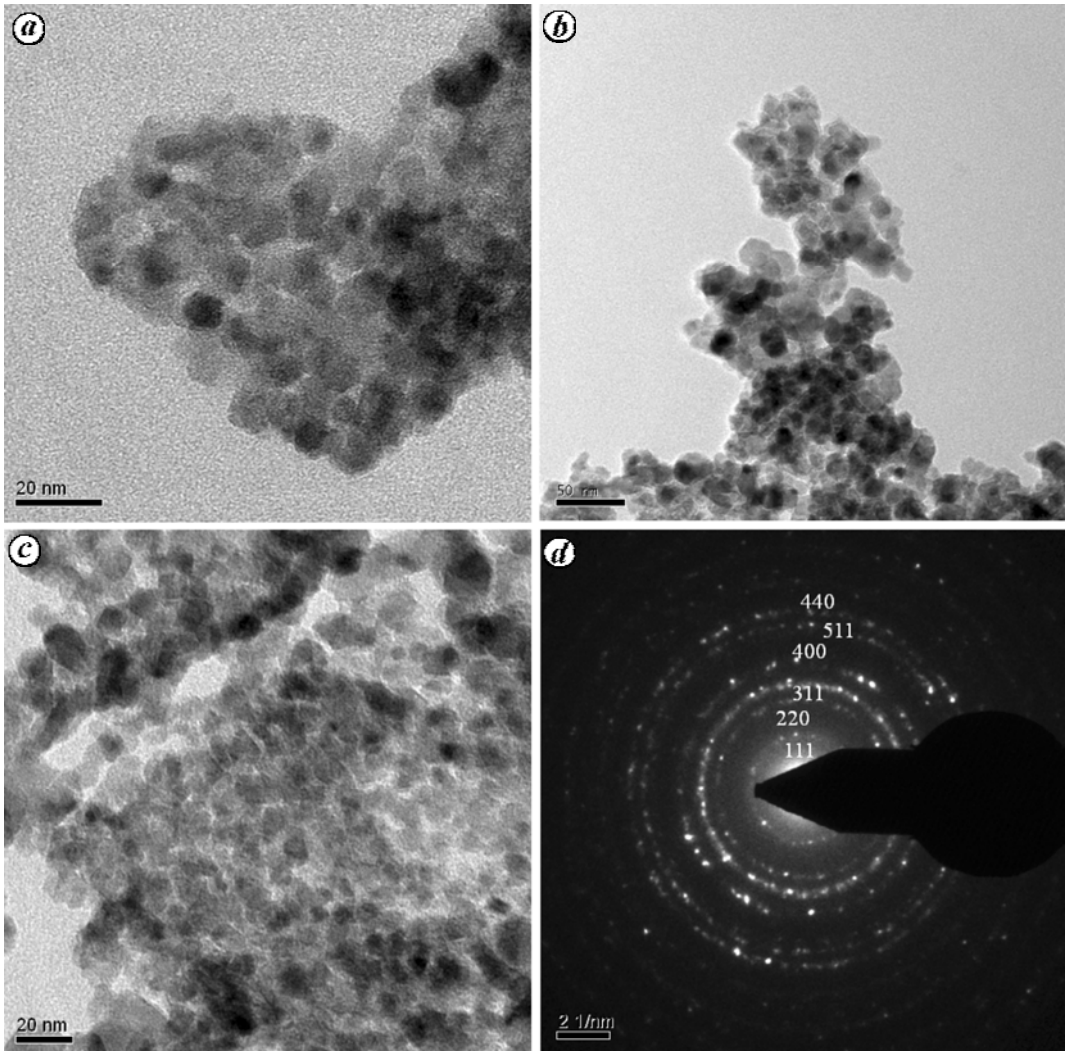

Figure 4. TEM images of the $NiMn_2O_4$ sample prepared at different temperatures: (***a***) 400°C, (***b***) 450°C, (***c***) 500°C and (***d***) selected area electron diffraction pattern at 500°C (indexing was based on a cubic $NiMn_2O_4$).

coupling). This would result in a much stronger canted antiferromagnetic behaviour for the Co-compound than compound **I**.

Thermal decomposition to mixed-metal oxides

As mentioned before, **I** was heated at different temperatures for 1 h and the resultant products were characterized by PXRD. Figure 3 shows the PXRD patterns of the products obtained after heating at 400°C, 450°C and 500°C. From the figure, it appears that the decomposed products are $NiMn_2O_4$ with a cubic structure (JCPDS 84-0542). If the particles are heated for a longer duration (~6 h) at 450°C and 500°C, we also observe the formation of $NiMnO_3$, which could be more stable (ESI, Figure S9; available online). The formation of $NiMnO_3$ during the synthesis of $NiMn_2O_4$ has been observed earlier[37]. The transient formation of $NiMn_2O_4$ suggests that both the $NiMnO_3$ and $NiMn_2O_4$ phases could be at equilibrium and the overall composition of the starting mixture could drive the formation of one of the phases over the other as a function of time and temperature. At low enough temperature (400°C), the formation of $NiMn_2O_4$ appears to be independent of the heating time and no $NiMnO_3$ phase was noted (ESI, Figure S10; available online). The average particle size of the spinel phase at each temperature was determined by fitting the (311) peak in the XRD pattern, using the Debye–Scherrer formula (Table 1)[38]. The spinel oxide appears to have small particle sizes, typically in the nano-regime. To know the exact shape and size of the $NiMn_2O_4$ particles, TEM studies were employed. These studies indicate that the particles are spherical in nature with the average particle size of 10, 15 and 18 nm for samples prepared at 400°C, 450°C and 500°C respectively. The particle sizes determined from the PXRD and TEM studies did not match completely. The TEM images of $NiMn_2O_4$ nanoparticles prepared at different tempera-

tures are shown in Figure 4. The selected area electron diffraction (SAED) pattern on a single particle obtained at 500°C is shown in Figure 4 *d*. The SAED pattern could be indexed to the cubic spinel $NiMn_2O_4$ phase. The TEM studies also indicate that there is a gradual increase in the average particle size with temperature. The N_2 adsorption studies were carried out using BELSORB-MAX at 77 K. The surface area of the samples heated at the three different temperatures was calculated using the BET adsorption isotherm (Figure 5). From the adsorption studies, it is clear that the surface area of the samples decreases with increase in the decomposition temperature (ESI, Figure S11, available online; Table 1). Similar behaviour has been observed earlier too[39].

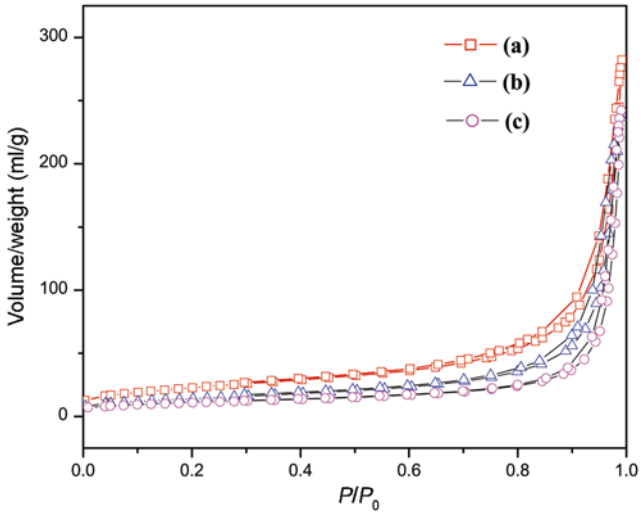

Figure 5. Nitrogen adsorption–desorption isotherms performed on nanoparticles of $NiMn_2O_4$ at 77 K: (***a***) 400°C (10 nm), (***b***) 450°C (15 nm) and (***c***) 500°C (18 nm).

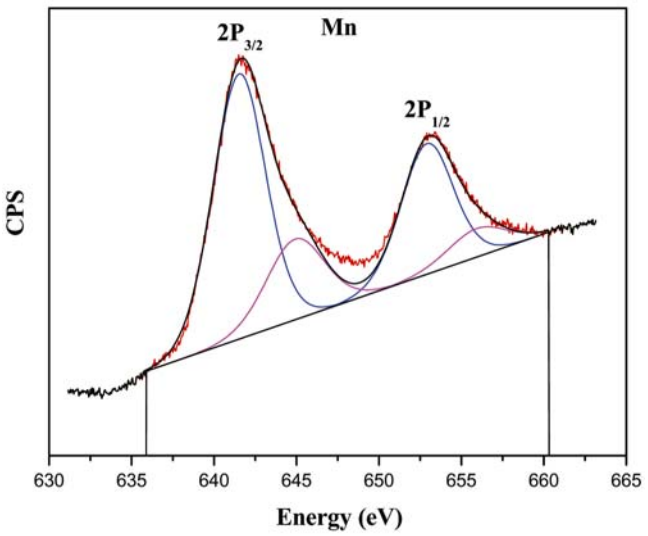

Figure 6. X-ray photoelectron spectroscopy analysis for manganese ion in $NiMn_2O_4$. CPS, Counts per second.

Magnetic properties of nanoparticles of $NiMn_2O_4$ spinel phases

The $NiMn_2O_4$ spinel phases prepared by the decomposition of **I** were studied for magnetic behaviour. The bulk $NiMn_2O_4$ needed for the characterization and comparison of magnetic behaviour was prepared by heating $NiMn_2O_4$ at 900°C/12 h.

Spinel oxides generally exhibit interesting magnetic behaviour. $NiMn_2O_4$ is known to exhibit ferromagnetic behaviour and the magnetic transition was explained using the strong overlap between the magnetic sublattices involving Ni^{2+} and Mn^{3+}. We have carried out X-ray photoelectron spectroscopy (XPS) studies on the sample to understand the nature of the oxidation state of Mn ions in our sample. It has been proposed that Mn can take Mn^{2+} and Mn^{4+} in spinel oxides. Our studies, however, clearly indicate only two distinct peaks corresponding to $2P_{3/2}$ and $2P_{1/2}$ at 641.5 and 653.1 eV along with the satellite bands at 645.1 and 656.3 eV respectively (Figure 6). This is in agreement with the previously observed values[40] for $NiMn_2O_4$. These are characteristic values for Mn ions in 3^+ oxidation state and suggest that we have only Mn^{3+} ions in our present compound. It has been known that in $NiMn_2O_4$ a small fraction of the Mn^{3+} ions can disproportionate to Mn^{2+} and Mn^{4+}. This would give rise to a formula[37,41] of $Ni^{2+}_{1-x}Mn^{2+}_x[Ni^{2+}_x\ Mn^{3+}_{2-2x}Mn^{4+}_x]O_4$.

The temperature variability of the magnetic susceptibility was measured employing a field of 50 Oe for both the bulk as well as the nanoparticles of $NiMn_2O_4$ (Figure 7). The magnetic behaviour suggests the onset of a magnetic transition at $T_C = \sim 118$ K for the bulk. Similar magnetic transitions have been observed at 100, 105 and 108 K respectively, for the 10, 15 and 18 nm particles of the $NiMn_2O_4$ phases. The observed transition temperatures for the various $NiMn_2O_4$ compounds are lower

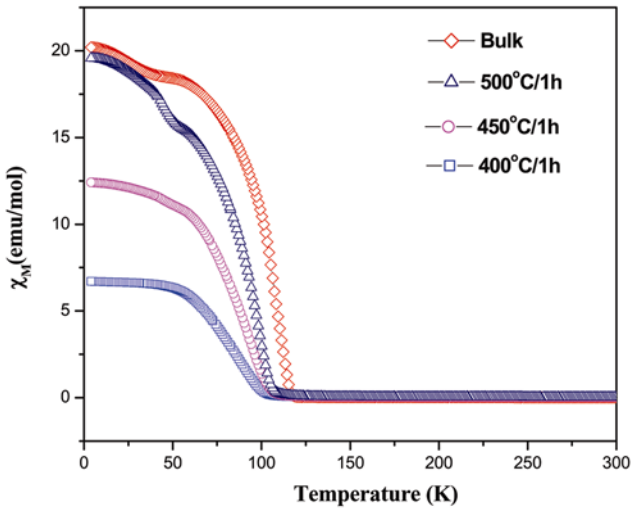

Figure 7. Temperature variation of the magnetic susceptibility, χ_M, using an applied field of $H = 50$ Oe for the $NiMn_2O_4$ nanoparticles and the bulk sample.

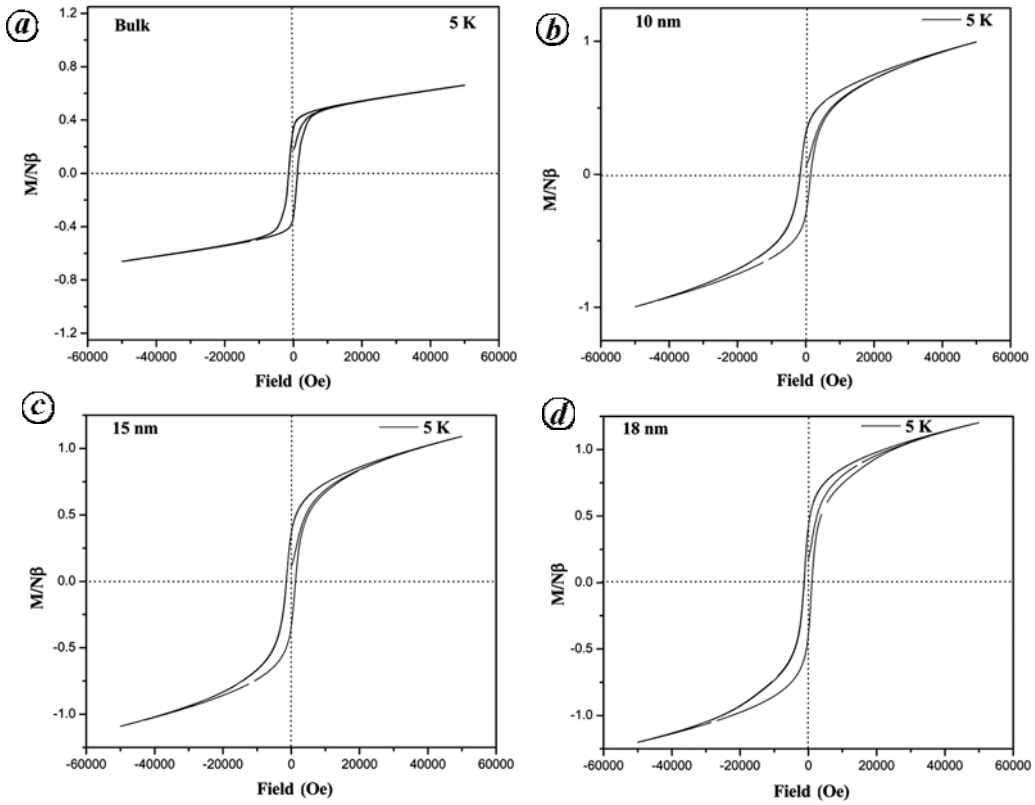

Figure 8. *M* versus *H* plot of the bulk sample (***a***) and the $NiMn_2O_4$ nanoparticles (***b***–***d***).

compared to the value of 145 K observed[41] for the single crystal of $NiMn_2O_4$. Similar variations in the magnetic ordering temperatures for the sintered $NiMn_2O_4$ have been observed earlier[42]. As can be noted, the magnetic transition temperature (T_C) exhibits a gradual decrease with the particle size, which could be due to the reduction of the crystallite sizes of the $NiMn_2O_4$ samples. The magnetic susceptibility data in the temperature range 200–300 K were fitted for the Curie–Weiss behaviour. The effective paramagnetic moment (μ_{eff}) values calculated did not exhibit any systematic trend as a function of the particle size. The calculated μ_{eff} values for the bulk and $NiMn_2O_4$ particles were in the range 6.65–6.77 μ_B. These values are in close agreement with the paramagnetic moment (μ_{eff}) observed[41] for the $NiMn_2O_4$ single crystal (6.9 μ_B).

Isothermal magnetization measurements, $M(H)$, were carried out both on the bulk and the various nanoparticles of $NiMn_2O_4$ (Figure 7). The $M(H)$ curves of the bulk sample recorded at 5 K indicate a hysteresis behaviour without the saturation, which also suggests the ferrimagnetic nature of the ordering (Figure 8). The $M(H)$ curve at 150 and 300 K is linear, which is in agreement with the paramagnetic state as inferred from the $M(T)$ curve (ESI, Figure S12; available online). The magnetization studies on the nanoparticles of $NiMn_2O_4$ (10, 15 and 18 nm) indicate that the magnetic behaviour is comparable with similar remnant field and coercivity.

Conclusions

Careful and selective replacement of the octahedral Mn^{2+} ions by Ni^{2+} ions in the MOF compound $[Mn_3\{C_6H_3(COO)_3\}_2]$ gives rise to the mixed-metal MOF, $[NiMn_2\{C_6H_3(COO)_3\}_2]$, **I**. Compound **I** acts as a single-source precursor for the formation of the ceramic spinel oxide, $NiMn_2O_4$, at temperatures around 400°C. HRTEM and PXRD studies suggest that the particle sizes of the $NiMn_2O_4$ phases are in the nanometre regime. Magnetic studies on the parent MOF **I** indicate antiferromagnetic interactions and a possible canting at low temperatures. The $NiMn_2O_4$ spinel phases exhibit a particle size-dependent magnetic ordering. This and other related studies clearly establish the possibility of employing mixed-metal MOF for the formation of important ceramic oxides. This opens up another avenue to pursue the use of this important family of compounds.

1. Gopalakrishnan, J. and Rao, C. N. R., *New Directions in Solid State Chemistry*, Cambridge University Press, 1995.
2. West, A. R., *Solid State Chemistry and its Application*, John Wiley, 2003.
3. Wells, A. F., *Structural Inorganic Chemistry*, Clarendon Press, Oxford, 1984.
4. Lavela, P., Tirado, J. L. and Abarca, C. V., Sol–gel preparation of cobalt manganese mixed oxides for their use as electrode materials in lithium cells. *Electrochim. Acta*, 2007, **52**, 7986–7995.
5. Chaves, A. C. *et al.*, Photoluminescence in disordered Zn_2TiO_4. *J. Solid State Chem.*, 2006, **179**, 985–992.

6. Song, X. Q. and Zhang, Z. J., Shape control and associated magnetic properties of spinel cobalt ferrite nanocrystals. *J. Am. Chem. Soc*., 2004, **126**, 6164–6168.
7. Yamasaki, Y., Miyasaka, S., Kaneko, Y., He, J.-P., Arima, T. and Tokura, Y., Magnetic reversal of the ferroelectric polarization in a multiferroic spinel oxide. *Phys. Rev. Lett*., 2006, **96**, 207204-1–207204-4.
8. Fujishiro, Y., Hamamoto, K., Shiono, O., Katayama, S. and Awano, M., Synthesis and thermoelectric characterization of polycrystalline $Ni_{1-x}Ca_xCo_2O_4$ (x = 0–0.05) spinel materials. *J. Mater. Sci.: Mater. Electron*., 2004, **15**, 769–773.
9. Johnston, D., Prakash, C., Zachariasen, H. W. H. and Viswanathan, R., High temperature superconductivity in the Li–Ti–O ternary system. *Mater. Res. Bull*., 1973, **8**, 777–784.
10. Akther Hossain, A. K. M., Seki, M., Kawai, T. and Tabata, H., Colossal magnetoresistance in spinel type $Zn_{1-x}Ni_xFe_2O_4$. *J. Appl. Phys*., 2004, **96**, 1273–1275.
11. Wolf, S. A. *et al.*, Spintronics: a spin-based electronics vision for the future. *Science*, 2001, **294**, 1488–1495.
12. Macklen, E. D., *Thermistors*, Electrochemical Publications, Glasgow, 1979.
13. Shenoy, S. D., Joy, P. A. and Anantharaman, M. R., Effect of mechanical milling on the structural, magnetic and dielectric properties of coprecipitated ultrafine zinc ferrite. *J. Magn. Magn. Mater*., 2004, **269**, 217–226.
14. Shaju, K. M. and Bruce, P. G., A stoichiometric nano-$LiMn_2O_4$ spinel electrode exhibiting high power and stable cycling. *Chem. Mater*., 2008, **20**, 5557–5562.
15. Spiers, H. *et al.*, Self-propagating high temperature synthesis of magnesium zinc ferrites ($Mg_xZn_{1-x}Fe_2O_3$): thermal imaging and time-resolved X-ray diffraction experiments. *J. Mater. Chem*., 2004, **14**, 1104–1111.
16. Yu, S. H., Fujino, T. and Yoshimura, M., Hydrothermal synthesis of $ZnFe_2O_4$ ultrafine particles with high magnetization. *J. Magn. Magn. Mater*., 2003, **256**, 420–424.
17. Bid, S. and Pradhan, S. K., Preparation of zinc ferrite by high-energy ball-milling and microstructure characterization by Rietveld's analysis. *Mater. Chem. Phys*., 2003, **82**, 27–37.
18. Mohai, I., Szepvolgyi, J., Bertoti, I., Mohai, M., Gubicza, J. and Ungar, T., Thermal plasma synthesis of zinc ferrite nanopowders. *Solid State Ionics*, 2001, **141**, 163–168.
19. Wu, Z., Okuya, M. and Kaneko, S., Spray pyrolysis deposition of zinc ferrite films from metal nitrates solutions. *Thin Solid Films*, 2001, **385**, 109–114.
20. Mahata, P., Sankar, G., Madras, G. and Natarajan, S., A novel sheet 4*f*–3*d* mixed-metal pyridine dicarboxylate: synthesis, structure, photophysical properties and its transformation to a perovskite oxide. *Chem. Commun*., 2005, 5787–14789.
21. Mahata, P., Aarthi, T., Madras, G. and Natarajan, S., Photocatalytic degradation of dyes and organics with nanosized $GdCoO_3$. *J. Phys. Chem. C*, 2007, **111**, 1665–1674.
22. Rocha, J., Carlos, L. D., Paz, F. A. A. and Ananias, D., Luminescent multifunctional lanthanides-based metal–organic frameworks. *Chem. Soc. Rev*., 2011, **40**, 926–940.
23. McKinlay, A. C., Morris, R. E., Horcajada, P., Férey, G., Gref, R., Couvreur, P. and Serre, C., BioMOFs: metal–organic frameworks for biological and medical applications. *Angew. Chem., Int. Ed. Engl*., 2010, **49**, 6260–6266.
24. D'Alessandro, D. M., Smit, B. and Long, J. R., Carbon dioxide capture: prospects for new materials. *Angew. Chem., Intl. Ed. Engl*., 2010, **49**, 6058–6082.
25. Themed issue: metal–organic frameworks. *Chem. Soc. Rev*., 2009, **38**, 1213–1504.
26. Song, Y.-F. and Cronin, L., Postsynthetic covalent modification of metal–organic framework (MOF) materials. *Angew. Chem., Int. Ed. Engl*., 2008, **47**, 4635–4637.
27. Tanabe, K. K. and Cohen, S. M., Postsynthetic modification of metal–organic frameworks – a progress report. *Chem. Soc. Rev*., 2011, **40**, 498–519.
28. Mahata, P., Sarma, D., Madhu, C., Sundaresen, A. and Natarajan, S., $CoMn_2O_4$ spinel from a MOF: synthesis, structure and magnetic studies. *Dalton. Trans*., 2011, **40**, 1952–1960.
29. Yan, B. B., Olmstead, M. M. and Maggard, P. A., Effect of spin-ladder topology on 2D charge ordering: toward new spin-antiferroelectric transitions. *J. Am. Chem. Soc*., 2007, **129**, 12646–12647.
30. Das, S., Kim, H. and Kim, K., Metathesis in single crystal: complete and reversible exchange of metal ions constituting the frameworks of metal–organic frameworks. *J. Am. Chem. Soc.*, 2009, **131**, 3814–3815.
31. Caskey, S. R. and Matzger, A. J., Selective metal substitution for the preparation of heterobimetallic microporous coordination polymers. *Inorg. Chem*., 2008, **47**, 7942–7944.
32. Mahata, P., Sen, D. and Natarajan, S., A three-dimensional metal–organic framework with a distorted kagome related layer showing canted antiferromagnetic behaviour. *Chem. Commun*., 2008, 1278–1280.
33. Le Bail, A., Duroy, H. and Fourquet, J. L., *Ab-initio* structure determination of $LiSbWO_6$ by X-ray powder diffraction. *Mater. Res. Bull*., 1988, **23**, 447–452.
34. Behera, J. N. and Rao, C. N. R., A Ni^{2+} (S = 1) kagome compound templated by 1,8-diazacubane. *J. Am. Chem. Soc*., 2006, **128**, 9334–9335.
35. Papoutsakis, D., Grohol, D. and Nocera, D. G., Magnetic properties of a homologous series of vanadium jarosite compounds. *J. Am. Chem. Soc*., 2002, **124**, 2647–2656.
36. Moriya, T., Anisotropic superexchange interaction and weak ferromagnetism. *Phys. Rev*., 1960, **120**, 91–98.
37. Tang, X., Manthiram, A. and Goodenough, J. B., $NiMn_2O_4$ revisited. *J. Less-Common Metals*, 1989, **156**, 357–368.
38. Patterson, A. L., The Scherrer formula for X-ray particle size determination. *Phys. Rev*., 1939, **56**, 978–982.
39. Ruihua, C., Shu, Y., Li, L., Zheng, M., Wang, X., Wang, A. and Zhang, T., Synthesis and characterization of high surface area molybdenum phosphide. *Appl. Catal. A: Gen*., 2007, **316**, 160–168.
40. Al-Sagheer, F. A. and Zaki, M. I., Synthesis and surface characterization of todorokite-type microporous manganese oxides: implications for shape-selective oxidation catalysts. *Micropor. Mesopor. Mater*., 2004, **67**, 43–52.
41. Asrink, S., Waskowska, A., Drodzd, M. and Talik, E., Physical properties and X-ray diffraction of a $NiMn_2O_4$ single crystal below and above the ferromagnetic transition at T = 145 K. *J. Phys. Chem. Solids*, 1997, **58**, 725–729.
42. Almeida, J. M. A., Meneses, C. T., de Menezes, A. S., Jardim, R. F. and Sasaki, J. M., Synthesis and characterization of $NiMn_2O_4$ nanoparticles using gelatin as organic precursor. *J. Magn. Magn. Mater*., 2008, **320**, e304–e307.

ACKNOWLEDGEMENTS. We thank the Council of Scientific and Industrial Research, New Delhi, for the award of a fellowship (D.S.) and a research grant (S.N.). S.N. thanks the Department of Science and Technology, New Delhi, for the award of a research grant and a RAMANNA fellowship.

Received 10 April 2012; revised accepted 26 September 2012